Geophysical Research Letters

RESEARCH LETTER
10.1029/2018GL078433

Meridional Shift of the Oyashio Extension Front in the Past 36 Years

Baolan Wu[1], **Xiaopei Lin**[1], **and Bo Qiu**[2]

[1]Physical Oceanography Laboratory/CIMST, Ocean University of China and Qingdao National Laboratory for Marine Science and Technology, Qingdao, China, [2]Department of Oceanography, University of Hawai'i at Mānoa, Honolulu, HI, USA

Key Points:
- Eastern OE front has moved poleward in the past 36 years from 1982 to 2017, but western front has no obvious shift
- Meridional shift of the eastern OE front is largely determined by the poleward movement of zero wind stress curl line
- West-east different pattern of the OE front shift is consistent with wind changes and anomalous Ekman heat transport

Supporting Information:
- Supporting Information S1

Correspondence to:
X. Lin,
linxiaop@ouc.edu.cn

Citation:
Wu, B., Lin, X., & Qiu, B. (2018). Meridional shift of the Oyashio extension front in the past 36 years. *Geophysical Research Letters*, *45*, 9042–9048. https://doi.org/10.1029/2018GL078433

Received 19 APR 2018
Accepted 5 JUL 2018
Accepted article online 11 JUL 2018
Published online 5 SEP 2018

©2018. American Geophysical Union. All Rights Reserved.

Abstract The meridional shift of Oyashio Extension (OE) front in the past 36 years was analyzed by using the high-resolution Optimum Interpolation SST data. The annual mean OE front has moved northward in its eastern part (between 157°E and 172°E) by 0.018°/year but no obvious poleward shift in the western OE front (between 145°E and 157°E). It is shown that the trade wind became stronger and broader, and the whole wind field moved northward in the past 36 years, shifting the zero wind stress curl line (or the zero Sverdrup streamline) and the eastern OE front northward. The above mechanism is confirmed by a 1.5-layer reduced-gravity model simulation as well as the altimetry data. Meanwhile, the local Ekman heat transport anomaly due to the wind field changes is found to be one of the contributors to the northward shift of the eastern OE front. However, both wind stress curl and local Ekman heat transport anomalies do not favor northward shift of the western OE front.

Plain Language Summary The Oyashio Extension (OE) front between the subtropical and subpolar ocean circulations is key region in the climate system with huge heat and mass transport variability, strong atmospheric storms, as well as major CO2 sinks. Ongoing efforts are being sought to understand the OE front variability in connection with climate change, but how its meridional shift under wind changes in the past several decades remain unclear. Here, we analyze the OE front shift from 1982-2017. Our results show that the eastern OE front shift northward with the zero wind stress curl line (zero Sverdrup stream line) moving northward, while the western OE front has no shift. The anomalous Ekman heat transport is also favorable for the west-east different shift of OE front. We believe that this work will appeal to the readers of GRL because it not only provides quantifications of the OE front shift based on high-resolution observations, but more importantly, also supplies new clues to the dynamic relationship between the OE front variability and the wind changes. When published, we believe our study will lead to improvement of climate prediction and projection especially in the ocean western boundary current regions, which is the most challenge area for modelling.

1. Introduction

In the midlatitude North Pacific, the western boundary current system including the Kuroshio and Oyashio Extensions (KOE) has been known as the most energetic region in the North Pacific. In the KOE region, there are two important fronts, the Kuroshio Extension (KE) front and the Oyashio Extension (OE) front. The KE front is highly baroclinic and is characterized by strong sea surface height gradient. In comparison, the OE front possesses little sea surface height features, due to strong density compensation between the temperature and salinity anomalies (e.g., Isoguchi et al., 2006; Yuan & Talley, 1996) but intense sea surface temperature (SST) and salinity gradients. Featured by its strong SST gradient, the meridional shift of OE front could generate enhanced SST anomaly (Pak et al., 2017) and affect the overlaying atmospheric circulation and storm activity (Frankignoul et al., 2012; Smirnov et al., 2015). Especially in the low frequency (interannual to decadal time scales), SST anomalies in the OE front are considered as the driven force of atmosphere variability (Masunaga et al., 2016; Revelard et al., 2016; Taguchi et al., 2012) and the North Pacific decadal climate change (Kwon et al., 2010; Nakamura et al., 1997; Nakamura & Yamagata, 1999; Qiu et al., 2017). The meridional shift of OE front has been in the past attributed to the basin-scale wind forcing (Kwon & Deser, 2007; Nonaka et al., 2006; Schneider et al., 2002; Seager et al., 2001) via the oceanic Rossby wave adjustment that modulates the latitude and strength of the OE front (Kwon et al., 2010; Nonaka et al., 2008).

Recently, Qiu et al. (2017) point out that rather than a single and continuous SST front, the OE front is composed of two independent systems. Specifically, two northeast-southwest-oriented OE fronts, the western OE

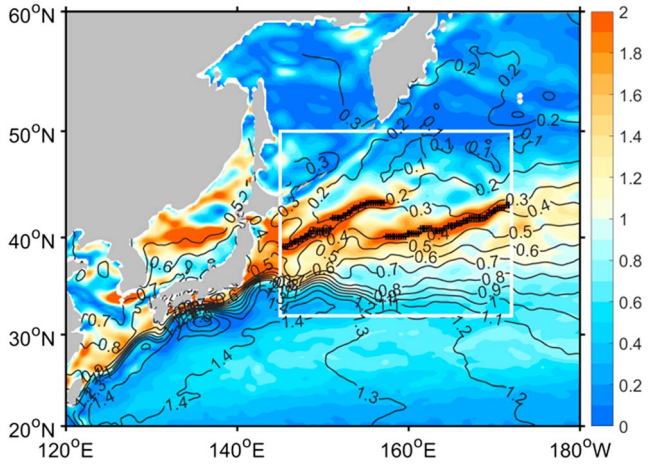

Figure 1. White box is the calculation area for OE front (32–50°N, 145–172°E). The black contours denote mean dynamic topography (MDT, unit: m), and the color shading denotes climatological meridional SST gradient (unit: °C per latitude). Black dots indicate the climatological position of the OE front including two independent parts: The western OE front (145–157°E) and the eastern OE front (157–172°E).

front between 145°E and 153°E and the eastern OE front between 153°E and 173°E, exist along the latitude band of 38–43°N. Similar features have been previously noted by Isoguchi et al. (2006) in their study of the surface OE. Given this spatial pattern of the OE front, does its meridional shift also exhibit west-east difference? The objective of this study is to address this particular question.

This paper is organized as follows. In section 2, we provide a brief description about the data and method used in this study. Section 3 shows the zonal-averaged meridional shift of the western and eastern OE fronts in the past 36 years. Section 4 analyzes the dynamics for the different OE front meridional shift in the western and eastern parts. Section 5 discusses the results and provides conclusions.

2. Data and Methodology

The SST data used in this study are based on the National Oceanic and Atmospheric Administration Optimum Interpolation SST (OISST) version 2 (Reynolds et al., 2007) that blended the Advanced Very High-Resolution Radiometer infrared satellite SST data, the Advanced Microwave Scanning Radiometer satellite SST data, and in situ temperature data from ships and buoy measurements. The optimally interpolated OISST data set has a spatial grid resolution of 0.25° and a temporal resolution of 1 day and covers the period from September 1981 to December 2017. We use the Ssalto/Duacs delayed time multimission maps of the absolute dynamic topography (ADT) distributed by AVISO over the 1993–2017 period with a monthly temporal resolution and 0.25° × 0.25° (latitude × longitude) spatial resolution. The wind data are from the European Centre for Medium-Range Forecast (ECMWF) Interim Reanalysis (Dee et al., 2011), hereafter ERA-I, supplied by the ECMWF. ERA-I wind data are available over 39 years from 1979 to 2017, but we choose the same period with the OISST during 1982–2017. The World Ocean Atlas 2013 climatology (WOA13, Locarnini et al., 2013; Zweng et al., 2013) temperature and salinity data from 1975 to 2012 are used to calculate the climatological mixed layer depth. Both ERA-I wind data and WOA13 data have a monthly temporal resolution and 1° × 1° (latitude × longitude) spatial resolution. Annual means are constructed from monthly means by averaging the data from January to December.

The OE front position in the North Pacific Ocean (32–50°N, 145–172°E) is defined by the maximum meridional SST gradient (dSST/d*y*) and separated into two independent frontal parts: western OE front (145–157°E) and eastern OE front (157–172°E) as shown in Figure 1. Similar to Qiu et al. (2017) who identify the OE front by specific contour value of 0.4-m ADT, we identify the OE front position with ADT equals to 0.3 m for the western OE front and 0.4 m for the eastern OE front as shown in Figure 1. Considering that the ADT will increase in a warming world with melting land ice, the ADT used in this study are detrended with 19 mm/year according to Chen et al. (2017). We also examine other choices of the ADT values which are near the maximum meridional SST gradient and found that the results are similar (figures not shown). We set up a 1.5-layer reduced-gravity model following Qiu and Lukas (1996; details in supporting information Text S1) to quantify the wind-forced OE front meridional shift. We use the layer thickness anomaly (LTA) from the model output equalling to −70 m to represent the position of the OE front. Due to the overshooting of the 1.5-layer model, the OE front defined by LTA has a systematic bias of about 4.5° northward displacement (see Figure S1).

Here SST anomalies are defined as the SST deviations from the annual climatology of 1982–2017. Wind stress and wind stress curl (WSC) anomalies are defined by the same way as the SST anomalies. We use a 5% significance level for all confidence coefficients, based on a two-tailed Student's *t* test in which the degrees of freedom are estimated by considering the lag-1 autocorrelation, calculated following Bretherton et al. (1999).

3. Zonal-Averaged Meridional Shifts of the Western and Eastern OE Fronts

To explore the annual mean meridional shift of the OE front, the time series of zonal-averaged western and eastern OE front positions are shown in Figure 2. We found clear difference in the OE front variability between the western and eastern parts. In the western OE front (Figure 2a), there is no northward shift by the SST

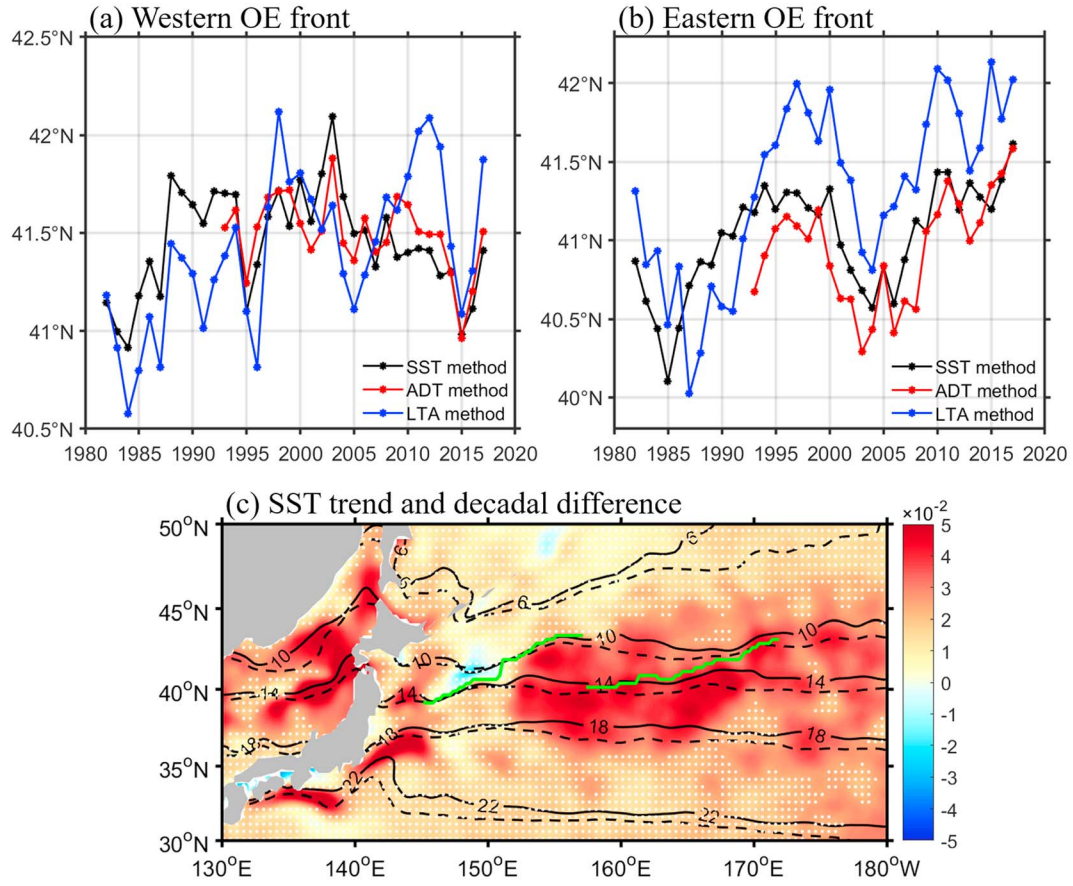

Figure 2. (a) Time series of the annual mean zonal-averaged meridional shift of the western OE front position. Black line is the OE front defined by the maximum meridional SST gradient (no obvious trend), red line for the specific contour value of absolute dynamic topography (*ADT* = 0.3 m, no obvious trend), and blue line for the specific contour value of the layer thickness anomaly (*LTA* = −70 m, 1982–2017: trend = 0.019 ± 0.012°/year, $P < 0.05$; 1993–2017: no obvious trend) from 1.5-layer model, respectively. *P* value smaller than 0.05 means that the trend is significant at the 95% confidence level. (b) Same as (a) but for the eastern OE front. Black line is the OE front defined by the maximum meridional SST gradient (1982–2017: trend = 0.018 ± 0.010°/year, $P < 0.05$; 1993–2017: trend = 0.013 ± 0.011°/year, $P < 0.05$), red line for the specific contour value of absolute dynamic topography (*ADT* = 0.4 m, 1993–2017: trend = 0.019 ± 0.014°/year, $P < 0.05$), and blue line for the specific contour value of the layer thickness anomaly (*LTA* = −70 m, 1982–2017: trend = 0.035 ± 0.030°/year, $P < 0.05$; 1993–2017: trend = 0.016 ± 0.012°/year, $P < 0.05$) from 1.5-layer model, respectively. (c) The color shading denotes SST trend (unit: °C/year) during 1982–2017. The black dashed and solid contours indicate the mean SST for 1982–1991 and 2008–2017, respectively (unit: °C). Green lines indicate the climatological position of the OE front. White dots indicate the trends are blow the 5% significance level. OE = Oyashio Extension; SST = sea surface temperature; ADT = absolute dynamic topography; LTA = layer thickness anomaly.

gradient method and only weak trend by the LTA method. Overall, similar interannual variability is captured by all three OE front definitions: the SST gradient method, the ADT method from altimetry data and the LTA method from model output. For the eastern OE front (Figure 2b), on the other hand, all the results from three methods show consistent northward shift. Even in the recent 25 years with the ADT observation (red line in Figure 2b), the eastern OE front still has an obvious poleward shift trend. Our results for the eastern OE front variability are similar with Pak et al. (2017) who use a high-resolution model to study the OE front shift. The eastern OE front position also shows strong decadal variability, and there are good correlations among these three definitions. For example, the eastern OE front was located in relatively low latitudes in early1980s and 2000s, while it migrated to higher latitudes during the early 1990s and 2010s. The different shift pattern between the western and eastern OE fronts can also be verified by the SST trend pattern shown in Figure 2c. SST warming is very robust in the eastern OE front region but nearly no warming in the western OE front area. This implies a northward shift of SST contours and the SST front in the eastern OE front as

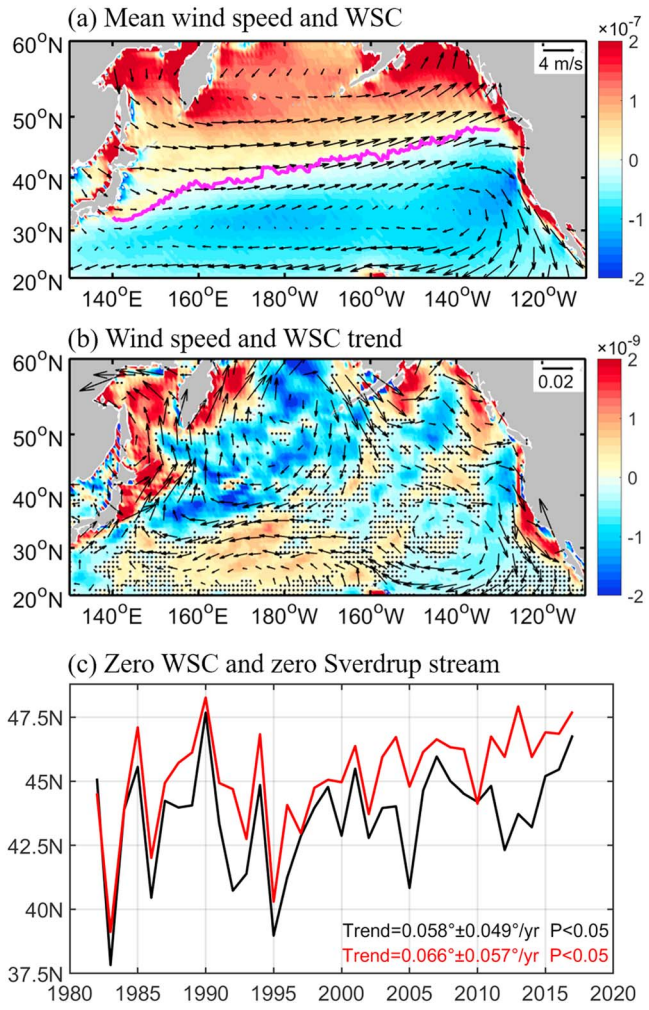

Figure 3. (a) Mean WSC (color shading, unit: N/m^3) and wind speed (vectors, unit: m/s) in the North Pacific Ocean during the period from 1982 to 2017. Magenta line indicates the climatology zero WSC position. (b) The trend of WSC (color shading, unit: N/m^3/year) and wind speed (vectors, unit: m/s/year) during 1982–2017. Black dots indicate that the trends are below the 5% significance level. (c) Time series of the annual mean zonal-averaged meridional shift of the zero WSC (black line, averaged over the North Pacific basin, 20–55°N, 140–130°W) and the zero Sverdrup stream line (red line, averaged over the OE front region, 32–50°N, 145–172°E) position from 1982 to 2017. *P* value smaller than 0.05 indicates that the trend is significant at the 5% significance level. WSC = wind stress curl.

revealed by the difference of SST contour positions between the two decades of 1982–1991 (black dashed lines) versus 2008–2017 (black solid lines) in Figure 2c.

It is worth noting that the 1.5-layer reduced-gravity model is purely driven by wind stresses without any thermodynamics. The good agreement of the OE front variability between the LTA method and the SST gradient method indicates that the wind-forced dynamics are primary for determining the OE front shift. If the wind forcing is dominant, the position of the OE front, or the confluence point between the wind-driven subtropical and subpolar gyres, can be estimated by the zero WSC line or more accurately the zero Sverdrup streamline. To test this hypothesis, we check the wind stress field changes in the past 36 years in Figure 3. Figure 3a presents the mean WSC and wind vector field. The OE front is located along ~41°N, at the northern area of the zero WSC line under prevailing westerlies forcing with a positive WSC. Figure 3b shows the trends of WSC and wind vector in the past 36 years. It is clear that the trade wind in the subtropics became stronger and broader, and the entire wind field moved northward, weakening the WSC in both the subtropical and subpolar oceans. Reflecting this movement by the entire subtropical wind field, Figure 3c reveals that the northward moving trend of the zonal-averaged zero WSC line (black line in Figure 3c) in the North Pacific basin (20–55°N, 140–130°W) is 0.058 ± 0.049°/year or about 2° from 1982 to 2017. This northward shift of zero WSC line causes a northward shift in zero Sverdrup streamline (red line in Figure 3c, zonal-averaged in the OE front region from 145°E to 172°E) and then the northward shift of the eastern OE front.

We should point out that the latitudinal change in the zonally averaged OE front is not as large as the zonally averaged zero WSC line. The northward shift of the eastern OE front is only about one third of the zero-curl line shift, and the interannual variability of the OE front (around 1.5°) is also much less than the interannual variability of the zero WSC line (around 10°). One possibility is the integration mechanism proposed by Qiu and Lukas (1996) with regard to the bifurcation of the North Equatorial Current off the Philippine coast. The seasonal movement of the North Equatorial Current bifurcation point is much less than that for the zero WSC line because the wind-forced oceanic changes integrate out along the path of baroclinic Rossby wave characteristics. This is the same in the OE front region. As shown in Figure S2, the LTA variability in the 1.5-layer model in the OE front region is much less than that derived by the Sverdrup theory. The reduced LTA variability would decrease meridional variability of the OE front.

4. Dynamics for the Different OE Front Meridional Shift in Western and Eastern Parts

The OE front shift is not uniform along the whole frontal region as shown in the last section, and this feature is clearer in Figure 4a, which shows the annual mean movement trend of the OE front position as a function of longitude. The OE front moves northward significantly only in the region east of 157°E (the eastern OE frontal area). West of 157°E (the western OE frontal area), the OE front exhibits no trend or even a weak southward trend in the past 36 years.

A relevant question to ask is why the OE front shift is different between its western and eastern parts. As we discussed in the preceding section, the position of OE front is determined by the wind forcing and can be estimated by the zero WSC or Sverdrup streamline. In our 1.5-layer reduced-gravity model results, the

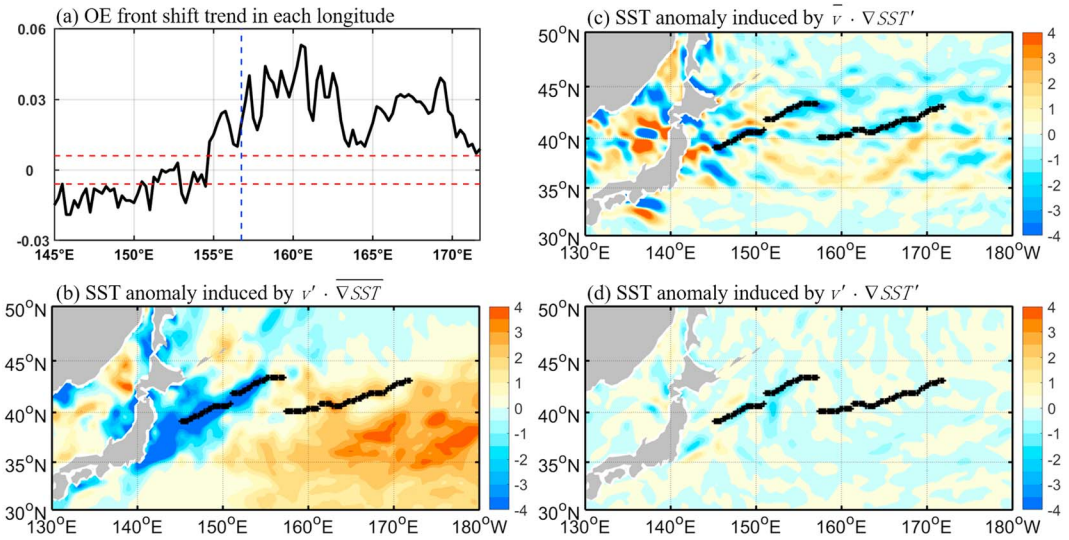

Figure 4. (a) The annual mean trend (unit: degrees latitude per year) of the OE front shift in each longitude from 145°E to 172°E during the period from 1982 to 2017. Blue dashed line denotes the 157°E longitude. Red dashed lines indicate the 5% significance level of the trend (±0.006 degrees of latitude per year). (b) SST anomalies caused by Ekman heat transport term $v' \cdot \overline{\nabla \mathrm{SST}}$ (unit: °C) and the black dots indicate the climatological OE front position. (c, d) Same as (b) but for $\bar{v} \cdot \nabla \mathrm{SST}'$ and $v' \cdot \nabla \mathrm{SST}'$ terms, respectively. OE = Oyashio Extension; SST = sea surface temperature.

LTA-defined OE front shows no shift in its western part and a northward shift in its eastern part. When we check the WSC trend as shown in Figure 3b, in the east of 157°E along the OE front latitudes, the WSC trend is nearly negative in every gird point and this will move the zero WSC line and then the eastern OE front northward. But in the west of 157°E near the boundary area, the WSC trend changes its sign to a positive value (see Figure 3b) and this works to cancel the northward shift of the OE front induced by the negative interior WSC trend.

Besides the wind forcing mentioned above, the local SST front position is also affected by local heat budget. For example, a stronger warming in the south of front would make SST contours more confined in the north of front and pushes the front northward as shown in Figure 2c.

To further explore the role of thermodynamics in contributing to the OE front shift, we analyze the upper ocean mixed layer heat budget that affects the local position of the OE SST front. The governing equation for SST can be written as

$$\frac{\partial \mathrm{SST}}{\partial t} = \frac{Q_{\mathrm{net}}}{c_p \rho H_m} - v \cdot \nabla \mathrm{SST} + R, \tag{1}$$

where Q_{net} is the net surface heat flux, c_p is the specific heat of seawater, ρ is the seawater density, and H_m is mixed layer depth estimated as the depth at which the water density is 0.125 kg/m^3 denser than at the sea surface (Monterey & Levitus, 1997). For simplicity, we only use the climatological value of H_m. The term $v \cdot \nabla \mathrm{SST}$ denotes the SST change caused by advection, and R is the residual. For more details, see Qiu and Kelly (1993).

We can decompose all variables into two parts

$$\mathrm{SST} = \overline{\mathrm{SST}} + \mathrm{SST}', \tag{2}$$

$$v = \bar{v} + v', \tag{3}$$

$$Q_{\mathrm{net}} = \overline{Q_{\mathrm{net}}} + Q'_{\mathrm{net}}, \tag{4}$$

$$R = \bar{R} + R', \tag{5}$$

where the $^{-}$ term denotes the mean value and the $'$ term, the deviation from the $^{-}$ term. Then the $v \cdot \nabla SST$ term can be decomposed into

$$v \cdot \nabla \mathrm{SST} = \overline{v} \cdot \overline{\nabla \mathrm{SST}} + v' \cdot \overline{\nabla \mathrm{SST}} + \overline{v} \cdot \nabla \mathrm{SST}' + v' \cdot \nabla \mathrm{SST}', \tag{6}$$

By assuming

$$\frac{\partial \overline{\mathrm{SST}}}{\partial t} = \frac{\overline{Q_{\mathrm{net}}}}{c_p \rho H_m} - \overline{v} \cdot \overline{\nabla \mathrm{SST}} + \overline{R} = 0, \tag{7}$$

we have

$$\frac{\partial \mathrm{SST}'}{\partial t} = \frac{Q'_{\mathrm{net}}}{c_p \rho H_m} - v' \cdot \overline{\nabla \mathrm{SST}} - \overline{v} \cdot \nabla \mathrm{SST}' - v' \cdot \nabla \mathrm{SST}' + R'. \tag{8}$$

Due to the limitations of observations, it is hard to conduct a thorough heat budget analysis in the OE front region. A recent study by Larson et al. (2018) found that the Ekman heat transport is an important component to the midlatitude SST variance in the KOE region (especially in prevailing westerlies) and controls the advection term. Following their study, we have evaluated the $v' \cdot \overline{\nabla \mathrm{SST}}$, $\overline{v} \cdot \nabla \mathrm{SST}'$ and $v' \cdot \nabla \mathrm{SST}'$ terms due to Ekman flows and found $v' \cdot \overline{\nabla \mathrm{SST}}$ is the dominant term (Figures 4b, 4c and 4d):

$$v' \cdot \overline{\nabla \mathrm{SST}} = U'_E \cdot \frac{\partial \overline{\mathrm{SST}}}{\partial x} + V'_E \cdot \frac{\partial \overline{\mathrm{SST}}}{\partial y} = \frac{\tau'_y}{f H_m \rho} \cdot \frac{\partial \overline{\mathrm{SST}}}{\partial x} - \frac{\tau'_x}{f H_m \rho} \cdot \frac{\partial \overline{\mathrm{SST}}}{\partial y}, \tag{9}$$

where f is the Coriolis parameter and τ'_y and τ'_x are the surface wind stress anomalies in the y and x directions, respectively.

Figure 4b shows the SST anomalies caused by the anomalous Ekman velocity ($v' \cdot \overline{\nabla \mathrm{SST}}$ term) in the past 36 years. In the western OE front region, cold Ekman heat transport tends to decrease SST in the south of the OE front, resulting in no obvious poleward shift in the western OE front (between 145°E and 157°E) as indicated by Figure 4a. In the eastern OE frontal region, warm Ekman heat transport increases the SST to the south of the OE front, shifting the front northward. The different pattern of the OE front's northward shift is, as such, possibly caused by the local Ekman heat transport induced by the anomalous Ekman velocity, in addition to the basin-scale wind forcing.

Recently, Mitsudera et al. (2018) demonstrated that the western OE front is anchored by bottom topography and this could be another reason for the stationarity of the western OE front, in accordance with our results. The previous study by Qiu et al. (2017) indicated that the decadal variability of the western OE front is mainly affected by the KE variability, while the eastern OE front is more controlled by the open ocean dynamics. In our study, the KE front has no northward shift in the past 36 years (see Figure S3), which is similar to the western OE front and consistent with the previous findings by Seo et al. (2014) and Pak et al. (2017). This may imply that even in the longer time scales, the KE has an important effect on the western OE front but little impact on the eastern OE front.

5. Conclusion

We studied the meridional shift of the OE front in the past 36 years. The zonal-averaged frontal movement has a significant northward shifting trend of 0.018°/year (with the SST gradient method) from 1982 to 2017 in the eastern OE front (157°E to 172°E) but no obvious shift in the western OE front (145°E to 157°E). Similar trends are obtained with the use of other front identification methods. Dynamically, this northward shift of the eastern OE front is consistent with the northward shift of the zonal-averaged zero WSC or the zero Sverdrup streamline. The west-east different wind changes (positive WSC trend west of 157°E and negative WSC trend east of 157°E) in the past 36 years result in the different shift pattern of the western and eastern OE fronts. Thermodynamically, the west-east different pattern of the OE front shift agrees with the Ekman heat transport induced by anomalous Ekman velocity. Our study suggests that the OE front movement, or the subtropical and subpolar circulation variability, is controlled by the surface wind changes both via dynamic and thermodynamic processes. Due to the limitations of the available observations, our study

could only show the results for the recent three decades. With the increase in greenhouse gas emission, the extent to which the OE front will move under the global warming scenario needs further future explorations.

Acknowledgments
This study benefitted from discussions with Xianyao Chen and guidance of modeling from Hanshi Wang. Constructive comments made by two anonymous reviewers have significantly improved an early version of the manuscript. The Reynolds OISST data used in this study were accessed from ftp://eclipse.ncdc.noaa.gov/, the ERA-I wind data from http://apps.ecmwf.int/, the WOA13 data from https://www.nodc.noaa.gov/, and the SSH data from http://www.aviso.oceanobs.com. Source data for 1.5-layer model are available at Ocean and Atmosphere Data Center of Ocean University of China (coadc.ouc.edu.cn). Xiaopei Lin is supported by the China's national key research and development projects (2016YFA0601803), the National Natural Science Foundation of China (41490641, 41521091, and U1606402), and the Qingdao National Laboratory for Marine Science and Technology (2017ASKJ01).

References

Bretherton, C. S., Widmann, M., Dymnidov, V. P., Wallace, J. M., & Blade, I. (1999). The effective number of spatial degrees of freedom of a time-varying field. *Journal of Climate*, *12*(7), 1990–2009. https://doi.org/10.1175/1520-0442(1999)012%3C1990:TENOSD%3E2.0.CO;2

Chen, X., Zhang, X., Church, J. A., Watson, C. S., King, M. A., Monselesan, D., et al. (2017). The increasing rate of global mean sea-level rise during 1993–2014. *Nature Climate Change*, *7*(7), 492–495. https://doi.org/10.1038/nclimate3325

Dee, D. P., Uppala, S. M., Simmons, A. J., Berrisford, P., Poli, P., Kobayashi, S., et al. (2011). The ERA-Interim reanalysis: Configuration and performance of the data assimilation system. *Quarterly Journal of the Royal Meteorological Society*, *137*(656), 553–597. https://doi.org/10.1002/qj.828

Frankignoul, C., Sennechael, N., Kwon, Y. O., & Alexander, M. A. (2012). Influence of the meridional shifts of the Kuroshio and the Oyashio extensions on the atmospheric circulation. *Journal of Climate*, *24*(3), 762–777. https://doi.org/10.1175/2010JCLI3731.1

Isoguchi, O., Kawamura, H., & Oka, E. (2006). Quasi-stationary jets transporting surface warm waters across the transition zone between the subtropical and the subarctic gyres in the North Pacific. *Journal of Geophysical Research*, *111*, c10003. https://doi.org/10.1029/2005JC003402

Kwon, Y.-O., Alenxader, M. A., Bond, N. A., Frankignoul, C., Nakamura, H., Qiu, B., & Thompson, L. (2010). Role of the Gulf Stream and Kuroshio-Oyashio systems in large-scale atmosphere-ocean interaction: A review. *Journal of Climate*, *23*(12), 3249–3281. https://doi.org/10.1175/2010JCLI3343.1

Kwon, Y.-O., & Deser, C. (2007). North Pacific decadal variability in the Community Climate System Model version 2. *Journal of Climate*, *20*(11), 2416–2433. https://doi.org/10.1175/JCLI4103.1

Larson, S. M., Vimont, D. J., Clement, A. C., & Kirtman, B. P. (2018). How momentum coupling affects Sst variance and large-scale pacific climate variability in CESM. *Journal of Climate*, *31*(7), 2927–2944. https://doi.org/10.1175/JCLI-D-17-0645.1

Locarnini, R. A., Mishonov, A. V., Antonov, J. I., Boyer, T. P., Garcia, H. E., Baranova, O. K., et al. (2013). World Ocean Atlas 2013, volume 1: Temperature. S. Levitus, Ed., A. Mishonov technical Ed.; NOAA atlas NESDIS 73, 40 pp.

Masunaga, R., Nakamura, H., Miyasaka, T., Nishii, K., & Qiu, B. (2016). Interannual modulations of oceanic imprints on the wintertime atmospheric boundary layer under the changing dynamical regimes of the Kuroshio Extension. *Journal of Climate*, *29*(9), 3273–3296. https://doi.org/10.1175/JCLI-D-15-0545.1

Mitsudera, H., Miyama, T., Nishigaki, H., Nakanowatari, T., Nishikawa, H., Nakamura, T., et al. (2018). Low ocean-floor rises regulate subpolar sea surface temperature by forming baroclinic jets. *Nature Communications*, *9*(1), 1190. https://doi.org/10.1038/s41467-018-03526-z

Monterey, G. I., & Levitus, S. (1997). Seasonal variability of mixed layer depth for the world ocean. *NOAA Atlas NESDIS*, *14*, 96.

Nakamura, H., Lin, G., & Yamagata, T. (1997). Decadal climate variability in the North Pacific during the recent decades. *Bulletin of the American Meteorological Society*, *78*(10), 2215–2225. https://doi.org/10.1175/1520-0477(1997)078%3C2215:DCVITN%3E2.0.CO;2

Nakamura, H., & Yamagata, T. (1999). Recent decadal SSST variability in the northwestern Pacific and associated atmospheric anomalies. In A. Navarra (Ed.), *Beyond El Niño: Decadal and Interdecadal Climate Variability* (pp. 49–62). Berlin Heidelberg: Springer.

Nonaka, M., Nakamura, H., Tanimoto, Y., & Kagimoto, T. (2008). Interannual-to-decadal variability in the Oyashio and its influence on temperature in the subarctic frontal zone: An eddy-resolving OGCM simulation. *Journal of Climate*, *21*(23), 6283–6303. https://doi.org/10.1175/2008JCLI2294.1

Nonaka, M., Nakamura, H., Tanimoto, Y., Kagimoto, T., & Dasaki, H. (2006). Decadal variability in the Kuroshio-Oyashio Extension simulated in an eddy-resolving OGCM. *Journal of Climate*, *19*(10), 1970–1989. https://doi.org/10.1175/JCLI3793.1

Pak, G., Park, Y. H., Vivier, F., Badie, R. B., Garric, G., & Chang, K. I. (2017). Upper-ocean thermal variability controlled by ocean dynamics in the Kuroshio-Oyashio Extension region. *Journal of Geophysical Research: Oceans*, *122*, 1154–1176. https://doi.org/10.1002/2016JC012076

Qiu, B., Chen, S., & Schneider, N. (2017). Dynamical links between the decadal variability of the Oyashio and Kuroshio Extensions. *Journal of Climate*, *30*(23), 9591–9605. https://doi.org/10.1175/JCLI-D-17-0397.1

Qiu, B., & Kelly, K. A. (1993). Upper ocean heat balance in the Kuroshio Extension region. *Journal of Physical Oceanography*, *23*(9), 2027–2041. https://doi.org/10.1175/1520-0485(1993)023%3C2027:UOHBIT%3E2.0.CO;2

Qiu, B., & Lukas, R. (1996). Seasonal and interannual variability of the North Equatorial Current, the Mindanao Current and the Kuroshio along the Pacific western boundary. *Journal of Geophysical Research*, *101*(C5), 12315–12330. https://doi.org/10.1029/95JC03204

Revelard, A., Frankignoul, C., Sennechael, N., Kwon, Y.-O., & Qiu, B. (2016). Influence of the decadal variability of the Kuroshio Extension on the atmospheric circulation in the cold season. *Journal of Climate*, *29*(6), 2123–2144. https://doi.org/10.1175/JCLI-D-15-0511.1

Reynolds, R. W., Smith, T. M., Liu, C., Chelton, D. B., Casey, K. S., & Schlax, M. G. (2007). Daily high-resolution-blended analyses for sea surface temperature. *Journal of Climate*, *20*(22), 5473–5496. https://doi.org/10.1175/2007JCLI1824.1

Schneider, N., Miller, A. J., & Pierce, D. W. (2002). Anatomy of North Pacific decadal variability. *Journal of Climate*, *15*(6), 586–605. https://doi.org/10.1175/1520-0442(2002)015%3C0586:AONPDV%3E2.0.CO;2

Seager, R., Kushnir, Y., Naik, N. H., Cane, M. A., & Miller, J. (2001). Wind-driven shifts in the latitude of the Kuroshio-Oyashio extension and generation of SST anomalies on decadal timescales. *Journal of Climate*, *14*(22), 4249–4265. https://doi.org/10.1175/1520-0442(2001)014%3C4249:WDSITL%3E2.0.CO;2

Seo, Y., Sugimoto, S., & Hanawa, K. (2014). Long-term variations of the Kuroshio Extension path in winter: Meridional movement and path state change. *Journal of Climate*, *27*(15), 5929–5940. https://doi.org/10.1175/JCLI-D-13-00641.1

Smirnov, D., Newman, M., Alexander, M. A., Kwon, Y. O., & Frankignoul, C. (2015). Investigating the local atmospheric response to a realistic shift in the Oyashio sea surface temperature front. *Journal of Climate*, *28*(3), 1126–1147. https://doi.org/10.1175/JCLI-D-14-00285.1

Taguchi, B., Nakamura, H., Komori, N., Kuwano-Yoshida, A., Takaya, K., & Goto, A. (2012). Seasonal evolutions of atmospheric response to decadal SST anomalies in the North Pacific subarctic frontal zone: Observations and a coupled model simulation. *Journal of Climate*, *25*(1), 111–139. https://doi.org/10.1175/JCLI-D-11-00046.1

Yuan, X. J., & Talley, L. D. (1996). The subarctic frontal zone in the North Pacific: Characteristics of frontal structure from climatological data and synoptic surveys. *Journal of Geophysical Research*, *101*(C7), 16491–16508. https://doi.org/10.1029/96JC01249

Zweng, M. M., Reagan, J. R., Antonov, J. I., Locarnini, R. A., Mishonov, A. V., Boyer, T. P., et al. (2013). World Ocean Atlas 2013, volume 2: Salinity. S. Levitus, Ed., A. Mishonov Technical Ed.; NOAA Atlas NESDIS 74, 39 pp.